

Experimental characterisation of unsharp qubit measurements in a semi-device-independent setting

Hammad Anwer,¹ Sadiq Muhammad,¹ Walid Cherifi,¹ Nikolai Miklin,² Armin Tavakoli,³ and Mohamed Bourennane¹

¹Department of Physics, Stockholm University, S-10691 Stockholm, Sweden

²Institute of Theoretical Physics and Astrophysics, National Quantum Information Center, Faculty of Mathematics, Physics and Informatics, University of Gdansk, 80-952 Gdansk, Poland

³Département de Physique Appliquée, Université de Genève, CH-1211 Genève, Switzerland

Unsharp measurements are increasingly important in quantum information theory and tests of quantum theory. Here, in a semi-device-independent setting, we experimentally demonstrate their noise-robust characterisation while only assuming that the involved devices operate on qubits and that the detected events constitute a fair sample. Our experiment involves three parties; the first party prepares a qubit system, the second party performs operations which returns both a classical and quantum outcome and the latter is measured by the third party. From the measured probabilities we show nearly-optimal quantum correlations for unsharp observables, falsify every model in which the operations are simulated with stochastic projective qubit measurements and obtain narrow intervals to which the sharpness parameter can be confined. Moreover, we also certify two sequential pairs of incompatible measurements and quantify their degree of incompatibility. Finally, we discuss our characterisation of the sharpness parameter as compared to that obtained from a tomographic scheme subjected to small errors.

Introduction.— Textbook measurements in quantum theory are represented by complete sets of orthogonal projectors. However, general measurements in quantum theory are described by positive operator-valued measures (POVMs), i.e. an ordered set of positive operators $\{M_i\}_i$ with normalisation $\sum_i M_i = \mathbb{1}$. Evidently, standard projective measurements are instances of POVMs but not all POVMs are projective measurements. These non-projective measurements are foundationally interesting and relevant to many phenomena and applications of quantum theory. Due to Neumark's theorem [1], every non-projective measurement can be modelled as a projective measurement applied jointly to a target system and an ancilla. Such purification of non-projective measurements is the typical method for laboratory implementations. This fact highlights that the notion of non-projectiveness is meaningfully applied only to fixed degrees of freedom.

Some non-projective measurements, of are extremal in the space of all POVMs with fixed Hilbert space dimension and number of outcomes i.e. they cannot be simulated with stochastic implementation of other measurements [2]. Whereas such POVMs have been studied in broad contexts [2–10], far from all non-projective measurements are of this type. In fact, many interesting POVMs are *unsharp* measurements, in the sense that they are weaker (noisy) variants of projective measurements. These measurements enable an experimenter to control the information-disturbance trade-off by suitably tuning the unsharpness (degree of noise) of the measurements [11]. A maximal unsharpness corresponds to a non-interactive measurement, which neither extracts information from, nor disturbs, the incoming state. A minimal unsharpness corresponds to a sharp (rank-one projective) measurement, which induces a maximal disturbance in the state in exchange for extracting a large (if not maximal) amount of information. In the intermediate cases, unsharp measurements extract a restricted amount of information while maintaining some degree of coherence. This makes them broadly relevant. Key examples include the study of weak measurements [12], continuous noisy measurements [13], quantum random number generation [14], tests of the memory-capacity of classi-

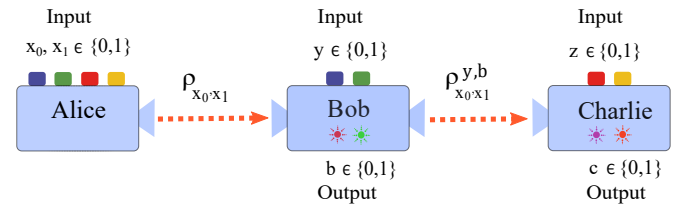


FIG. 1: Alice receives two bits x_0, x_1 and sends the qubit state ρ_{x_0,x_1} to Bob who receives an input y and produces a classical output b and a quantum output $\rho_{x_0,x_1}^{y,b}$ which is measured by Charlie according to his input z , yielding an outcome c .

cal systems [15] and the sharing of various forms of quantum correlations [11, 16–18]. This has recently led to a number of experiments focused on the implementation of incompatible measurements [19–21], quantum contextuality [18] and quantum nonlocality [22–24].

All this motivates the importance of characterising and certifying properties of unsharp measurements in laboratories. Quantum devices can be characterised already in simple experiments in which one party prepares states and another party measures them [25, 26]. However, such experiments are not suitable for characterising unsharp measurements since it is possible to simulate their outcome statistics with stochastic projective measurements. Recently, this conceptual obstacle has been overcome [27, 28] by introducing a third party: the state prepared by the first party is sent to a second party who implements an operation that produces both a classical and quantum output, the latter of which is relayed to a third party who performs a measurement (see Figure 1). The key idea is that strong correlations between the first two parties requires fairly sharp measurements, which cause a large disturbance that ensures weaker correlations between the first and third party. Importantly if the unsharp measurement of the second party is not genuine, in the sense that it is stochastically simulated with projective measurements, this will influence the quantum output and be detectable in the outcome statistics of the third party. In Refs [27, 28] the characterisation

is achieved semi-device-independently; by only assuming the Hilbert space dimension of the physical system. This assumption is often experimentally justifiable and also necessary in order to avoid the possibility of measurement purification (as discussed earlier).

In this Letter, we experimentally characterise unsharp measurements on the polarisation state of photons in a semi-device-independent setting. Ranging from small to large unsharpness parameters, we demonstrate nearly-optimal quantum correlations that both outperform any (stochastic) projective qubit measurements and certify a narrow interval to which the initially uncharacterised sharpness parameter can be confined. We then discuss how our semi-device-independent characterisation of unsharpness compares, in terms of assumptions, experimental complexity and accuracy, to that obtained via more commonplace tomographic methods. Finally, whereas previous experiments have demonstrated sequential pairs of measurements that are incompatible [18–23], we show that our data also allows us to quantify the degree of incompatibility [29] between two sequential pairs of incompatible measurements in a semi-device-independent setting.

Scenario and theoretical background.— Based on Refs. [27, 28], we describe the semi-device-independent scenario in the experiment. It involves three parties, Alice, Bob and Charlie (see Figure 1). Alice receives an input $x \equiv x_0, x_1 \in \{0, 1\}$ and prepares some uncharacterised qubit state denoted ρ_x , which she sends to Bob. Bob receives an input $y \in \{0, 1\}$ and performs a corresponding operation on ρ_x . This operation produces a classical output $b \in \{0, 1\}$ and some post-operation qubit state denoted $\rho_x^{y,b}$, which is sent to Charlie. Charlie receives an input $z \in \{0, 1\}$ and then measures $\rho_x^{y,b}$, yielding an outcome $c \in \{0, 1\}$. All inputs (x, y, z) are statistically independent and uniformly distributed. The limit of many rounds yields a probability distribution $p(b, c|x, y, z)$.

The probability distribution is used for a task known as a quantum random access code (QRAC) [30–32]. In a QRAC, a sender must encode two bits into one qubit which is sent to a receiver who attempts to randomly extract either the value of the first or second bit of the sender. In our scenario, two QRACs are considered simultaneously; one between Alice and Bob, and one between Alice and Charlie. Thus, the former is successful whenever $b = x_y$ and the latter is successful whenever $c = x_z$. The success probabilities in the two QRACs read

$$\begin{aligned} W_{AB} &= \frac{1}{8} \sum_{x,y} P(b = x_y|x, y), \\ W_{AC} &= \frac{1}{8} \sum_{x,z} P(c = x_z|x, z). \end{aligned} \quad (1)$$

Note that we can always take $W_{AB}, W_{AC} \in [\frac{1}{2}, 1]$. Evidently, W_{AB} is independent of Charlie. However, W_{AC} is not independent of Bob because he operates on the system before it reaches Charlie. Thus, his potentially disturbing influence will affect Charlie’s outcome statistics. The pair of witnesses (W_{AB}, W_{AC}) will be used to semi-device-independently characterise the unsharpness of Bob’s measurements.

Bob’s two operations ($y = 0, 1$) are described by the notion of a quantum instrument [33], which captures both the measurement statistics and the evolution of the measured state. A quantum instrument is defined as an ordered set of trace-non-increasing completely positive maps $\{\Lambda_{b|y}\}_b$ with the property that for any state ρ it holds that $p(b|y) = \text{tr}(\Lambda_{b|y}(\rho))$. Having observed the classical output b , the quantum output of the instrument is given by $\rho^{y,b} = \Lambda_{b|y}(\rho) / \text{tr}(\Lambda_{b|y}(\rho))$. Since we consider qubits and Bob has binary outcomes, the extremal quantum instruments may be written as $\Lambda_{b|y}(\rho) = K_{b|y} \rho K_{b|y}^\dagger$, where $\{K_{b|y}\}_b$ are Kraus operators satisfying $\sum_b K_{b|y}^\dagger K_{b|y} = \mathbb{1}$, with the convenient property that $K_{b|y}^\dagger K_{b|y} = B_{b|y}$ where $\{B_{b|y}\}_b$ are the two POVMs of Bob [34]. For simplicity, we can represent Bob’s POVMs in terms of two observables which in general read $B_y \equiv B_{0|y} - B_{1|y} = \alpha_y \mathbb{1} + \vec{n}_y \cdot \vec{\sigma}$, where \vec{n}_y are Bloch vectors, $\vec{\sigma}$ are the Pauli matrices and $|\alpha_y| \leq 1 - |\vec{n}_y|$. The sharpness of Bob’s POVMs is defined as $\eta_y = |\vec{n}_y|$. Notice that for $\eta_y \in \{0, 1\}$, the POVMs are non-interactive and sharp respectively, whereas $\eta_y \in (0, 1)$ corresponds to intermediate cases. We consider the case of $\eta \equiv \eta_0 = \eta_1$. It is worth emphasising that one can stochastically simulate Bob’s unsharp POVMs using only projective measurements, but one cannot simulate his quantum instrument in this manner. In other words, projective measurements can account for Bob’s outcome statistics but not for his post-measurement states. By considering both the classical and quantum output, we can distinguish a projective simulation from a genuine unsharp measurement.

The sharpness parameter η can be characterised by inspecting the witnesses (W_{AB}, W_{AC}) . Refs. [27, 28] showed that for a given value of W_{AB} , the optimal value of W_{AC} in quantum theory is given by

$$W_{AC} = \frac{1}{8} \left(4 + \sqrt{2} + \sqrt{16W_{AB} - 16W_{AB}^2 - 2} \right), \quad (2)$$

and that such an optimal pair implies a precise value of η . However, in the experimentally realistic case in which perfectly optimal quantum correlations are not relevant, a sub-optimal witness pair can be used to deduce upper and lower bounds on η ,

$$\begin{aligned} \eta &\geq \sqrt{2} (2W_{AB} - 1), \\ \eta &\leq 2\sqrt{(2 + \sqrt{2} - 4W_{AC})(2W_{AC} - 1)}. \end{aligned} \quad (3)$$

Thus, the closer the experimentally observed correlations are to the optimal ones in Eq. (2), the narrower is the interval to which we can confine the sharpness η . Note that for optimal quantum correlations, the upper and lower bounds are equal.

Experiment.— The optimal quantum correlations (2) are obtained with a unique quantum strategy (up to a global unitary) [27]. Alice needs to prepare four states forming a square on a great circle on the Bloch sphere. For simplicity we choose xz -plane and Alice’s four states $|\psi_{x_0x_1}\rangle = \cos \alpha_{x_0x_1} |0\rangle + \sin \alpha_{x_0x_1} |1\rangle$ corresponding to the four values $\{\frac{\pi}{8}, -\frac{3\pi}{8}, \frac{9\pi}{8}, \frac{5\pi}{8}\}$ of $\alpha_{x_0x_1}$ respectively, where $\rho_x =$

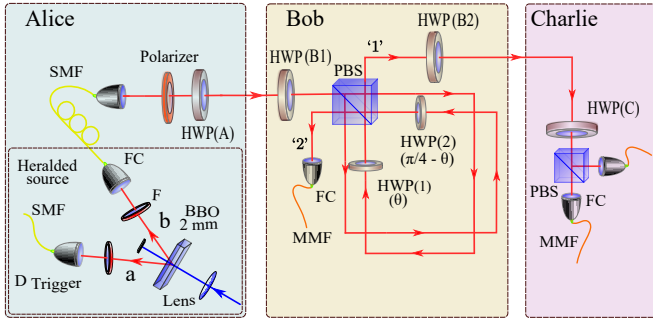


FIG. 2: Experimental setup. Alice prepares her states using a heralded photon source, a polariser and a half-wave plate HWP(A). Bob's instrument is realised by a shifted Sagnac interferometer where the sharpness parameter $\eta = \cos(4\theta)$ is tuned using half-wave plates HWP(1) and HWP(2). HWP(B1) and HWP(B2) are used to switch between the observables B_0 and B_1 as well as selecting the output corresponding to the outcome $b = 0$ and $b = 1$. Charlie performs projective (sharp) measurements on the received qubit from Bob using a HWP(C) and a polarisation beam splitter (PBS).

$|\psi_{x_0 x_1}\rangle\langle\psi_{x_0 x_1}|$. Similarly, the optimal quantum instruments of Bob correspond to the Kraus operators $K_{b|y} = \sqrt{(\mathbb{I} + (-1)^b B_y)/2}$ for a suitably chosen η , where $B_y \in \{\eta\sigma_x, \eta\sigma_z\}$ are the corresponding observables of Bob. The quantum output is sent to Charlie whose observables are two complementary projective measurements $C_0 = \sigma_x$ and $C_1 = \sigma_z$. In an ideal experiment, for every η , we obtain the witness pair,

$$W_{AB} = \frac{2 + \sqrt{2}\eta}{4}, \quad W_{AC} = \frac{4 + \sqrt{2} + \sqrt{2 - 2\eta^2}}{8}, \quad (4)$$

which satisfies the optimality condition (2).

We implemented this optimal strategy, using single-photon polarisation qubits where the computational basis corresponds to horizontal (H) and vertical (V) polarisation, i.e. $|H\rangle \equiv |0\rangle$ and $|V\rangle \equiv |1\rangle$. The complete optical setup is shown in Figure 2. Alice's preparation device also encloses a heralded single photons source that produces photons at wave-length 780 nm through spontaneous parametric down conversion (SPDC) by pumping a type-I beta barium borate (BBO) single crystal of thickness 2 mm using 390 nm femto-second laser pulses. Time correlated idler and signal photons are spectrally and spatially purified by passing through 3 nm (FWHM) wide optical filters (F) and coupling into single mode fibers (SMF) respectively. The idler photons in mode 'a' are detected by an avalanche photo-diode (APD), marked as D_{Trigger} , with detection efficiency $\sim 60\%$, which produces a trigger signal indicating the presence of a photon in mode 'b'. Alice prepares this photon in one of the four desired states $|\psi_{x_0, x_1}\rangle$ using a polariser when it only passes through $|H\rangle$ and a half-wave plate, HWP(A), at angles 11.25° , -11.25° , 33.75° and -33.75° respectively and sends it to Bob.

Bob's unsharp measurements on the received photons are performed using shifted Sagnac interferometer as described in [18, 23]. In this setup the strength of the measurement is controlled by rotating half-wave plate HWP(1) to θ and

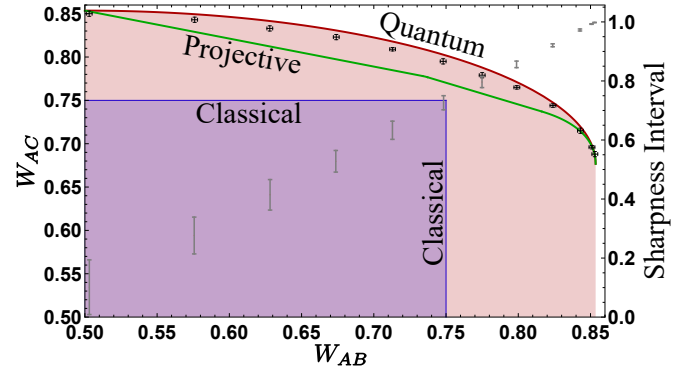


FIG. 3: Experimental results. Optimal quantum correlations (Red), optimal quantum correlations from stochastic projective measurements (Green), optimal classical correlations (Blue) and experimentally obtained values of witness pairs (W_{AB}, W_{AC}) (Black). The characterisation of the sharpness parameter η is depicted by gray bars corresponding to the interval to which it is confined (y-axis on the right-hand-side).

HWP(2) to $\frac{\pi}{4} - \theta$, that are placed respectively in the path of horizontally and vertically polarised beams after the polarisation beam splitter (PBS) such that $\eta = \cos(4\theta)$. To switch between the bases B_y according to the input y , Bob rotates both his wave-plates HWP(B1) and HWP(B2) to 22.5° and 0° respectively. The outcome of these measurements $b \in \{0, 1\}$ is encoded in the output path of the interferometer such that $b = 0$ ($b = 1$) corresponds to the detection of the photon in the output path '1' \equiv transmission ('2' \equiv reflection). In a sequential scenario, we choose to consider only one output path at a time to simplify the setup and by adding an additional rotation to the HWP(B1) and HWP(B2), we can select the output we want to analyse at a given time. Using output '2', Bob will locally be able to learn the outcome of his measurement counterfactually when using perfect detectors. Also, when the fair sampling assumption is invoked, which is the case in this experiment, Bob can still infer his outcome of the measurement locally using average photon rates.

Finally, Charlie's projective measurement setup is consisted of HWP(C), PBS, a pair of fiber couplers (FC) and multi-mode fibers (MMF) that propagate the photons to a pair of APDs. He performs $C_z \in \{\sigma_x, \sigma_z\}$ on the received qubits according to his random input $z \in \{0, 1\}$, by rotating HWP(C) to 22.5° and 0° respectively. The results of Charlie's marginal probabilities (for evaluating W_{AC}) are obtained by averaging out the inputs and outputs of Bob.

Results.— To evaluate (W_{AB}, W_{AC}) from the data, we require the marginal probabilities appearing in Eq (1). All parties setting are set using motorised rotation stages that are controlled by a computer program. To gather sufficient statistics we measure 60 sec in each setting with a rate of ~ 20 kHz and collected at least 1.2 million events. Each measured value of (W_{AB}, W_{AC}) together with the (black colour) error bars (horizontal and vertical corresponding to W_{AB} and W_{AC} respectively) is shown in Figure 3 and can be compared to the optimal quantum correlations (red colour) and the optimal classical correlations (blue colour, given by $W_{AB} \leq 3/4$ and

$W_{AC} \leq 3/4$). Our obtained quantum correlations are nearly optimal for all considered values of η . Also, in the worst case, the classical limit is outperformed by at least 15 standard deviations. Moreover, the data reliably outperforms the optimal quantum correlations attainable when Bob uses stochastic projective measurements (green colour) (see Ref [28]). This qualitatively certifies that the quantum instrument performs as desired. Notably, the projective bound is not outperformed for the two data points corresponding to $\eta \in \{0, 1\}$ since in these cases the bound coincides with the optimal quantum correlations.

From the inequalities in Eq (3), we can determine an upper and a lower bound on the sharpness parameter. Thus η can be confined to an interval for each of the measured values of the witness pair (W_{AB}, W_{AC}) . These certified intervals are depicted by gray bars in Figure 3 located vertically from the corresponding witness' and using the y-axis on the right side. We observe that the certification is more precise (the interval is smaller) as the sharpness parameter increases. The smallest (largest) interval, corresponding to an essentially projective (non-interactive) measurement, has a width of about 10^{-3} (0.2). This is due to the fact that the bounds in Eq (3) become more sensitive to small imperfections when W_{AC} increases. Further details about the experimental data is presented in Appendix.

Data Analysis.— The experiment is influenced by systematic errors originating from, for instance, imperfect waveplates as well as offsets in their marked zero position, finite PBS extinction and cross-talk, and limited interference visibility. The magnitude of these errors is revealed by the extent to which the experimental points are shifted away from the optimal quantum correlations. In order to minimise systematic errors, we carefully select and characterise all the optical components. This brings us closer to the optimal quantum correlation and the experimental points correspond to a more than 98% total visibility estimation. Nevertheless, random errors due to Poissonian statistics or due to repetition of the experimental settings with limited precision will spread the observed point on the Figure 3 to a region contained within the black bars. To keep this error low, all the settings are set by computerised controlled motors with repetition precision $< 0.02^\circ$. Errors together with mean values are provided in Appendix.

Quantifying sequential measurement incompatibility.— In order to witness quantum correlations, one requires incompatible measurements. In that sense, violating the classical constraint with W_{AB} (W_{AC}) certifies that Bob's (Charlie's) two POVMs are incompatible [35, 36]. It is, however, more informative to consider a quantitative inference; is it possible, by only considering (W_{AB}, W_{AC}) , to determine a lower bound on the extent to which Bob's and Charlie's POVMs are incompatible? In order to achieve such semi-device-independent quantification of Heisenberg uncertainty, one must first define a measure of incompatibility valid for dichotomic qubit observables. We use the *degree of incompatibility* introduced in Ref [29];

$$D(\vec{n}_0, \vec{n}_1) = |\vec{n}_0 + \vec{n}_1| + |\vec{n}_0 - \vec{n}_1| - 2, \quad (5)$$

where \vec{n}_0 and \vec{n}_1 are the Bloch vectors of the observables. All compatible observables obey $D \leq 0$ whereas incompatible observables obey $D \leq 2(\sqrt{2} - 1)$. As expected, the bound is saturated by two Pauli observables. In Appendix, we show that a given QRAC value, $W \in \{W_{AB}, W_{AC}\}$, implies the following lower bound on the degree of incompatibility,

$$D \geq 8W - 6. \quad (6)$$

Thus, whenever a QRAC exceeds the classical bound of $W = 3/4$, this certifies a degree of incompatibility. Applying Eq (6) separately to W_{AB} and W_{AC} , we find that for small η , Bob does not certify incompatibility whereas Charlie does so, and vice versa for large η . However, for some intermediate values of η , both W_{AB} and W_{AC} exceed the classical bound and thus we can quantify the incompatibility of two sequential pairs of measurements. For example, the experimental point $(W_{AB}, W_{AC}) = (0.775, 0.779)$ certifies that $D_B \geq 0.2$ and $D_C \geq 0.23$.

Comparison to tomographic scheme.— We have semi-device-independently characterised the sharpness parameter η . How does this compare to what can be obtained from a more standard characterisation method? For instance, one may consider a setting in which we can simplify the experiment by dispensing with Charlie: let a sender probe a measurement device with various preparations. We must now assume that the measurement device has no internal source of randomness (otherwise an unsharp POVM can be simulated projectively). Moreover, taking a tomographic approach, we can reconstruct the unsharp observable by assuming that the preparation device is trusted [37].

However, no preparation device is flawless. In Appendix, we consider a simple error-bounded tomographic model in which the sender prepares four states that, up to a fidelity of $1 - \epsilon$, form a tetrahedron on the Bloch sphere. We choose $\epsilon = 1\%$ and numerically consider how the estimated η may differ from its actual value. We find that the estimate can grow less precise for larger values of η , which is opposite to what we found in our experiment (see Figure 3). In comparison, for fairly strong measurements, we find that our experimental results are roughly an order of magnitude more precise than what can be guaranteed from the tomographic scheme. The advantage decreases as η decreases and vanishes roughly when $\eta \approx 0.35$. Thus, at the price of introducing Charlie in the experiment, we avoid making additional assumptions while also obtaining more precise characterisations for most values of η . We note that one could also consider more sophisticated tomographic methods, but this is beyond the scope of our work. Finally, we remark that small errors can significantly undermine the analogous task of state tomography [38].

Conclusions.— We demonstrated semi-device-independent characterisation of quantum instruments realising unsharp qubit measurements by performing sequential operations on an ensemble of qubits, obtaining nearly-optimal quantum correlations in two sequential QRACs. This also allowed us to falsify every quantum model based on stochastic projective measurements. Moreover, we used the sequential QRACs to determine lower bounds on the degree of incompatibility

in two sequential pairs of POVMs. Finally, we compared the precision of our characterisation of the sharpness parameter to that guaranteed in a simple tomographic scheme with small preparation errors and found that for most values of the sharpness parameter, the semi-device-independent characterisation obtains more precise results under weaker assumptions. Our results demonstrate the usefulness and practical feasibility of characterising unsharp measurements under weak assumptions.

Acknowledgements

This work was supported by the Swedish research council, Knut and Alice Wallenberg Foundation and the Swiss National Science Foundation (Starting grant DIAQ, NCCR-QSIT). NM acknowledges the financial support by the First TEAM Grant No. 2016-1/5.

-
- [1] M. A. Nielsen and I. L. Chuang, *Quantum Computation and Quantum Information*, 10th Anniversary Edition, Cambridge University Press (2011).
 - [2] G. M. D'Ariano, P. L. Presti, and P. Perinotti, Classical randomness in quantum measurements, *J. Phys. A: Math. Gen.* **38**, 5979 (2005).
 - [3] S. M. Barnett and S. Croke, Quantum state discrimination, *Advances in Optics and Photonics* **1**, 238 (2009).
 - [4] R. Derka, V. Bužek and A. K. Ekert, Universal Algorithm for Optimal Estimation of Quantum States from Finite Ensembles via Realizable Generalized Measurement, *Phys. Rev. Lett.* **80**, 1571 (1998).
 - [5] J. M. Renes, R. Blume-Kohout, A. J. Scott and C. M. Caves, Symmetric informationally complete quantum measurements, *Journal of Mathematical Physics* **45**, 2171 (2004).
 - [6] J. B. Brask, A. Martin, W. Esposito, R. Houlmann, J. Bowles, H. Zbinden, N. Brunner, Megahertz-Rate Semi-Device-Independent Quantum Random Number Generators Based on Unambiguous State Discrimination, *Phys. Rev. Applied* **7**, 054018 (2017).
 - [7] E. S. Gómez, et al., Device-Independent Certification of a Non-projective Qubit Measurement, *Phys. Rev. Lett.* **117**, 260401 (2016).
 - [8] A. Tavakoli, D. Rosset and M-O. Renou, Enabling computation of correlation bounds for finite-dimensional quantum systems via symmetrisation, *Phys. Rev. Lett.* **122**, 070501 (2019)..
 - [9] J. M. Renes, Spherical-code key-distribution protocols for qubits, *Phys. Rev. A* **70**, 052314 (2004).
 - [10] M. Oszmaniec, L. Guerini, P. Wittek, and A. Acín, Simulating Positive-Operator-Valued Measures with Projective Measurements, *Phys. Rev. Lett.* **119**, 190501 (2017).
 - [11] R. Silva, N. Gisin, Y. Guryanova and S. Popescu, Multiple Observers Can Share the Nonlocality of Half of an Entangled Pair by Using Optimal Weak Measurements, *Phys. Rev. Lett.* **114**, 250401 (2015).
 - [12] Y. Aharonov, D. Z. Albert and L. Vaidman, How the result of a measurement of a component of the spin of a spin-1/2 particle can turn out to be 100, *Phys. Rev. Lett.* **60**, 1351 (1988).
 - [13] A. A. Clerk, M. H. Devoret, S. M. Girvin, F. Marquardt, R. J. Schoelkopf, Introduction to quantum noise, measurement, and amplification, *Rev. Mod. Phys.* **82**, 1155 (2010).
 - [14] F. J. Curchod, M. Johansson, R. Augusiak, M. J. Hoban, P. Wittek and A. Acín, Unbounded randomness certification using sequences of measurements, *Phys. Rev. A* **95**, 020102(R) (2017)
 - [15] A. Tavakoli and A. Cabello, Quantum predictions for an unmeasured system cannot be simulated with a finite-memory classical system, *Phys. Rev. A* **97**, 032131 (2018).
 - [16] A. Bera, S. Mal, A. Sen(De) and U. Sen, Witnessing bipartite entanglement sequentially by multiple observers, *Phys. Rev. A* **98**, 062304 (2018).
 - [17] A. Shenoy H., S. Designolle, F. Hirsch, R. Silva, N. Gisin and N. Brunner, Unbounded sequence of observers exhibiting Einstein-Podolsky-Rosen steering, *Phys. Rev. A* **99**, 022317 (2019).
 - [18] H. Anwer, N. Wilson, R. Silva, S. Muhammad, A. Tavakoli and M. Bourennane, Noise-robust preparation contextuality shared between any number of observers via unsharp measurements, [arXiv:1904.09766](https://arxiv.org/abs/1904.09766).
 - [19] F. Piacentini, A. Avella, M. P. Levi, M. Gramegna, G. Brida, I. P. Degiovanni, E. Cohen, R. Lussana, F. Villa, A. Tosi, F. Zappa and M. Genovese, Measuring Incompatible Observables by Exploiting Sequential Weak Values, *Phys. Rev. Lett.* **117**, 170402 (2016).
 - [20] Y. Kim, Y-S. Kim, S-Y. Lee, S-W. Han, S. Moon, Y-H. Kim and Y-W. Cho, Direct quantum process tomography via measuring sequential weak values of incompatible observables, *Nature Communications* **9**, 192 (2018).
 - [21] J-S. Chen, M-J. Hu, X-M. Hu, B-H. Liu, Y-F. Huang, C-F. Li, C-G. Guo and Y-S. Zhang, Experimental realization of sequential weak measurements of non-commuting Pauli observables, *Optics Express* **27**, 6089 (2019).
 - [22] M. Schiavon, L. Calderaro, M. Pittaluga, G. Vallone, and P. Villoresi, Three-observer Bell inequality violation on a two-qubit entangled state, *Quantum Sci. Technol.* **2** 015010 (2017).
 - [23] M-J. Hu, Z-Y. Zhou, X-M. Hu, C-F. Li, G-C. Guo, and Y-S. Zhang, Observation of non-locality sharing among three observers with one entangled pair via optimal weak measurement, *npj Quantum Information* **4**, 63 (2018).
 - [24] G. Foletto, L. Calderaro, A. Tavakoli, M. Schiavon, F. Picciariello, A. Cabello, P. Villoresi and G. Vallone, Experimental Demonstration of Sustained Entanglement and Nonlocality After Sequential Measurements, [arXiv:1906.07412](https://arxiv.org/abs/1906.07412)
 - [25] A. Tavakoli, M. Smania, T. Vértesi, N. Brunner and M. Bourennane, Self-testing non-projective quantum measurements in prepare-and-measure experiments, [arXiv:1811.12712](https://arxiv.org/abs/1811.12712)
 - [26] A. Tavakoli, J. Kaniewski, A. Vértesi, D. Rosset and N. Brunner, Self-testing quantum states and measurements in the prepare-and-measure scenario, *Phys. Rev. A* **98**, 062307 (2018).
 - [27] K. Mohan, A. Tavakoli and N. Brunner, Sequential random access codes and self-testing of quantum measurement instruments, *New J. Phys.* **21** 083034 (2019).
 - [28] N. Miklin, J. J. Borkala and M. Pawłowski, Self-testing of unsharp measurements, [arXiv:1903.12533](https://arxiv.org/abs/1903.12533)
 - [29] P. Busch, P. Lahti and R. F. Werner, Heisenberg uncertainty for qubit measurements, *Phys. Rev. A* **89**, 012129 (2014).
 - [30] A. Ambainis, A. Nayak, A. Ta-Shama and U. Varizani, in *Proceedings of 31st ACM Symposium on Theory of Computing*,

- pp. 376-383, 1999.
- [31] A. Ambainis, D. Leung, L. Mancinska and M. Ozols, Quantum Random Access Codes with Shared Randomness, [arXiv:0810.2937](#)
 - [32] A. Tavakoli, A. Hameedi, B. Marques and M. Bourennane, Quantum Random Access Codes using Single d-level Systems, *Phys. Rev. Lett.* **114**, 170502 (2015).
 - [33] T. Heinosaari, and M. Ziman, The Mathematical Language of Quantum Theory, Cambridge University Press, 2011.
 - [34] J-P. Pellonpää, Quantum instruments: I. Extreme instruments *J. Phys. A: Math. Theor.* **46** 025302 (2013).
 - [35] A. Tavakoli and R. Uola, Measurement incompatibility and steering are necessary and sufficient for operational contextuality, *Phys. Rev. Research* **2**, 013011 (2020)
 - [36] C. Carmeli, T. Heinosaari and A. Toigo, Quantum random access codes and incompatibility of measurements, [arXiv:1911.04360](#)
 - [37] R. Schmied, Quantum State Tomography of a Single Qubit: Comparison of Methods, *J. Mod. Opt.* **63**, 1744 (2016).
 - [38] D. Rosset, R. Ferretti-Schöbitz, J-D. Bancal, N. Gisin and Y-C. Liang, Imperfect measurements settings: implications on quantum state tomography and entanglement witnesses, *Phys. Rev. A* **86**, 062325 (2012).

Appendix A: Quantifying the degree of incompatibility from a quantum random access code

We use the Bloch sphere representation to write the qubit preparations as $\rho_x = (\mathbb{1} + \vec{a}_x \cdot \vec{\sigma})/2$ and the qubit observables as $M_y = \alpha_y \mathbb{1} + \vec{b}_y \cdot \vec{\sigma}$, where \vec{a}_x and \vec{b}_y are Bloch vectors and $|\alpha_y| \leq 1 - |\vec{b}_y|$. Then, we can write the QRAC as

$$W = \frac{1}{2} + \frac{1}{16} \sum_{x,y} (-1)^{x_y} \text{tr}(\rho_x M_y) \\ = \frac{1}{2} + \frac{1}{8} \left[\vec{r}_0 \cdot (\vec{b}_0 + \vec{b}_1) + \vec{r}_1 \cdot (\vec{b}_0 - \vec{b}_1) \right], \quad (\text{A1})$$

where we have defined

$$\vec{r}_z = \frac{\vec{a}_{0z} - \vec{a}_{1\bar{z}}}{2}, \quad (\text{A2})$$

where \bar{z} is the bitflip of z . Now, for a given pair of measurements, let us maximise the QRAC over the preparations of Alice. Evidently, her optimal choice is to align \vec{r}_0 with $(\vec{b}_0 + \vec{b}_1)$ and \vec{r}_1 with $(\vec{b}_0 - \vec{b}_1)$. This yields

$$\max_{\{\rho_x\}} W = \frac{1}{2} + \frac{1}{8} \left(|\vec{b}_0 + \vec{b}_1| + |\vec{b}_0 - \vec{b}_1| \right) \\ = \frac{1}{2} \left(1 + \frac{D(\vec{b}_0, \vec{b}_1) + 2}{4} \right), \quad (\text{A3})$$

where D is the degree of incompatibility defined in Eq. (5). Hence, for some arbitrary observed success probability in a QRAC, it therefore holds that

$$W \leq \frac{1}{2} \left(1 + \frac{D(\vec{b}_0, \vec{b}_1) + 2}{4} \right), \quad (\text{A4})$$

which is rearranged to

$$D(\vec{b}_0, \vec{b}_1) \geq 8W - 6. \quad (\text{A5})$$

Appendix B: Comparison to error-bounded detector tomography

There are many methods of performing qubit tomography (see e.g. Ref [37]). We focus on a particularly simple case of scaled direct inversion tomography for an unbiased qubit observable. We need to introduce a preparation device which is fully controlled, i.e. it is assumed to flawlessly prepare states. In general, one requires a tomographically complete set of preparations. A simple and unbiased choice of such preparations is four states that form a tetrahedron on the Bloch sphere. The corresponding Bloch vectors can be taken as

$$\vec{a}_1 = \frac{(1, 1, 1)}{\sqrt{3}}, \quad \vec{a}_2 = \frac{(1, -1, -1)}{\sqrt{3}} \\ \vec{a}_3 = \frac{(-1, 1, -1)}{\sqrt{3}}, \quad \vec{a}_4 = \frac{(-1, -1, 1)}{\sqrt{3}}, \quad (\text{B1})$$

and the states are denoted $\rho_x^{\text{ideal}} = 1/2(\mathbb{1} + \vec{a}_x \cdot \vec{\sigma})$. Since a general unbiased qubit observable reads $E^{\text{lab}} = \vec{n} \cdot \vec{\sigma}$, the probabilities $p_x = \text{tr}(\rho_x^{\text{ideal}} E^{\text{lab}})$ can be written as

$$\vec{p} = A \vec{n} \quad (\text{B2})$$

where A is the 4×3 matrix with rows $\vec{a}_1, \vec{a}_2, \vec{a}_3, \vec{a}_4$. Hence, given the observation \vec{p} , we can deduce the initially unknown observable by evaluating

$$\vec{n} = (A^T A)^{-1} A^T \vec{p}. \quad (\text{B3})$$

However, no realistic experiment can live up to the idealisation of fully controlled preparation devices. To make a more realistic model, we introduce an error parameter $\epsilon \in [0, 1]$ for the preparation device. We consider that the preparation device outputs the desired states (B1) with average fidelity

$$\frac{1}{4} \sum_{x=1}^4 F(\rho_x^{\text{ideal}}, \rho_x^{\text{lab}}) \geq 1 - \epsilon, \quad (\text{B4})$$

where ρ_x^{lab} are the de-facto states prepared in the experiment. Notably, since the target states are pure, we have that $F(\rho_x^{\text{ideal}}, \rho_x^{\text{lab}}) = \text{tr}(\rho_x^{\text{ideal}} \rho_x^{\text{lab}})$. Thus, the smaller we choose ϵ , the closer must the laboratory states be to the targeted (tetrahedron) states. Notice that for $\epsilon = 0$, we must have $\rho_x^{\text{lab}} = \rho_x^{\text{ideal}}$. The introduced error means that the observed probabilities now read $p_x = \text{tr}(\rho_x^{\text{lab}} E^{\text{lab}})$ which via Eq. (B3) will lead to a somewhat inaccurate estimate (\vec{n}^{est} , corresponding to E^{est}) of the de-facto observable (E^{lab} , with Bloch vector \vec{n}^{lab}). It may happen that \vec{n}^{est} is not a valid Bloch vector; in such cases we renormalise it by letting $\vec{n}^{\text{est}} \rightarrow \vec{n}^{\text{est}}/|\vec{n}^{\text{est}}|$.

To what extent can a given ϵ influence the accuracy of the tomography? We evaluate the accuracy of the tomography in terms of the fidelity between the outcome-zero operators of

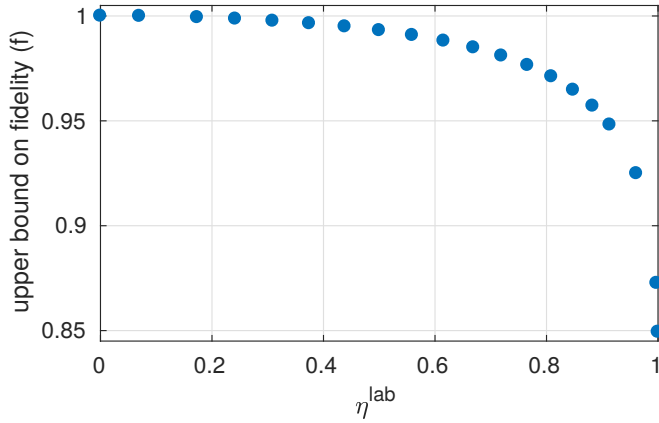


FIG. 4: Upper bound the fidelity $f(\epsilon, E^{\text{lab}})$ for $E^{\text{lab}} = \eta^{\text{lab}} \sigma_z$ in the detector tomography scheme using four tetrahedral states subject to $\epsilon = 1\%$ average error.

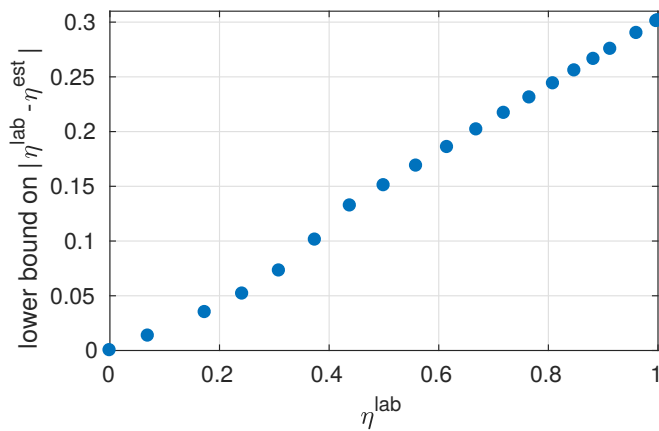


FIG. 5: Lower bound on the imprecision of the estimated sharpness of the laboratory observable $E^{\text{lab}} = \eta^{\text{lab}} \sigma_z$ in the detector tomography scheme using four tetrahedral states subject to $\epsilon = 1\%$ average error.

$E_0^{\text{lab}} = (\mathbb{1} + E^{\text{lab}})/2$ and $E_0^{\text{est}} = (\mathbb{1} + E^{\text{est}})/2$ ¹. Then, it is natural to consider the worst estimation compatible with the allowed error. This amounts to solving

$$f(\epsilon, E^{\text{lab}}) = \min_{\{\rho_x^{\text{lab}}\}} F(E_0^{\text{lab}}, E_0^{\text{est}}), \quad (\text{B5})$$

with $p_x = \text{tr}(\rho_x^{\text{lab}} E^{\text{lab}})$, the estimation performed via Eq. (B3) and the laboratory states obeying the constraint in Eq. (B4). We remark that the objective can be written on the simple form

$$F(E_0^{\text{lab}}, E_0^{\text{est}}) = \text{tr}(E_0^{\text{lab}} E_0^{\text{est}}) + 2\sqrt{\det(E_0^{\text{lab}}) \det(E_0^{\text{est}})}. \quad (\text{B6})$$

A reasonable choice of error, on par with that estimated to be present in our experiment in the main text, is $\epsilon = 1\%$. Fixing this error, we have numerically implemented the minimisation in Eq. (B5) for a laboratory observable of the form $E^{\text{lab}} = \eta^{\text{lab}} \sigma_z$. We performed the minimisation for several different values of η and the results are displayed in Figure 4. We see that as the observable becomes sharper, the impact of the error becomes greater. However, since the numerics are not guaranteed to find the global minimum, our results constitute upper bounds on $f(\epsilon, E^{\text{lab}})$. Thus, we run the risk of overestimating the guaranteed accuracy of the detector tomography scheme.

For every choice of η^{lab} , our numerics return the estimate E^{est} . We compute the sharpness (η^{est}) of this observable and consider how far it is from that of the targeted value (η^{lab}), i.e. we consider $|\eta^{\text{est}} - \eta^{\text{lab}}|$. The results are shown in Figure 5. In analogy with the fidelity, we find that the possible imprecision of the estimated sharpness parameter in the scheme increases with the sharpness of the observable. It is interesting to note that for a nearly-projective observable, an error of $\epsilon = 1\%$ is compatible with an estimated observable whose sharpness is between 25% – 30% incorrect.

TABLE I: Details of the results presented in Figure 3 of the main text, showing half-wave plates rotation θ used to tune the sharpness η of the Bob's effective measurement, its corresponding values, witness pair (W_{AB} , W_{AC}), certified sharpness (upper and lower bound) and sharpness interval together with their errors.

Half-wave-plate angle θ	Measurement Sharpness $\eta = \cos(4\theta)$	W_{AB}	W_{AC}	Sharpness Bound		Interval (Δ)
				Lower Bound	Upper Bound	
0	1.000	0.853 ± 0.002	0.688 ± 0.003	0.998 ± 0.006	1.00 ± 0.01	0.00 ± 0.01
2	0.990	0.851 ± 0.002	0.696 ± 0.002	0.992 ± 0.006	0.994 ± 0.008	0.00 ± 0.01
4	0.961	0.843 ± 0.002	0.715 ± 0.003	0.969 ± 0.006	0.98 ± 0.01	0.01 ± 0.01
6	0.914	0.824 ± 0.002	0.744 ± 0.002	0.916 ± 0.006	0.93 ± 0.01	0.01 ± 0.01
8	0.848	0.799 ± 0.002	0.765 ± 0.002	0.845 ± 0.006	0.87 ± 0.01	0.02 ± 0.01
10	0.766	0.775 ± 0.002	0.779 ± 0.003	0.778 ± 0.006	0.82 ± 0.02	0.04 ± 0.02
12	0.669	0.748 ± 0.002	0.795 ± 0.003	0.702 ± 0.006	0.75 ± 0.02	0.05 ± 0.02
14	0.559	0.713 ± 0.002	0.809 ± 0.002	0.602 ± 0.006	0.66 ± 0.02	0.06 ± 0.02
16	0.438	0.674 ± 0.002	0.823 ± 0.003	0.491 ± 0.006	0.56 ± 0.03	0.07 ± 0.03
18	0.309	0.628 ± 0.002	0.833 ± 0.003	0.363 ± 0.006	0.47 ± 0.03	0.10 ± 0.03
20	0.174	0.576 ± 0.002	0.843 ± 0.003	0.214 ± 0.006	0.34 ± 0.05	0.13 ± 0.05
22.5	0.000	0.503 ± 0.002	0.850 ± 0.003	0.009 ± 0.006	0.20 ± 0.01	0.2 ± 0.1